AIP Advances

Molecular dynamics simulations of the response of pre-damaged $SrTiO_3$ and $KTaO_3$ to fast heavy ions

Cite as: AIP Advances **10**, 015019 (2020); https://doi.org/10.1063/1.5133061
Submitted: 22 October 2019 . Accepted: 14 December 2019 . Published Online: 09 January 2020

Eva Zarkadoula, Yanwen Zhang, and William J. Weber

Molecular dynamics simulations of the response of pre-damaged $SrTiO_3$ and $KTaO_3$ to fast heavy ions

Cite as: AIP Advances 10, 015019 (2020); doi: 10.1063/1.5133061
Submitted: 22 October 2019 • Accepted: 14 December 2019 •
Published Online: 9 January 2020

Eva Zarkadoula,[1,a] Yanwen Zhang,[1] and William J. Weber[1,2]

AFFILIATIONS

[1] Materials Science and Technology Division, Oak Ridge National Laboratory, Oak Ridge, Tennessee 37831, USA
[2] Department of Materials Science and Engineering, University of Tennessee, Knoxville, Tennessee 37996, USA

[a] Electronic mail: zarkadoulae@ornl.gov

ABSTRACT

We investigate the energy dissipation and track formation due to ion irradiation in $SrTiO_3$ and $KTaO_3$. We use molecular dynamics simulations combined with the inelastic thermal spike model to simulate 21 MeV Ni ion irradiation in pristine and predamaged samples. The results are validated against experimental findings, showing that the level of initial disorder affects the electron-phonon interactions and the energy dissipation and deposition to the atoms. It is predicted that the ion track size increases linearly for low disorder levels, while its size saturates for high levels of disorder.

Ion irradiation can cause unwanted damage, for instance, in nuclear applications or space devices, but it is also a very useful tool in material modification and material design. Highly energetic ion beams deposit energy primarily to the electrons of the target material via the electronic energy loss mechanism, resulting in their excitation. Low energy ions interact primarily with the nuclei of the target via the nuclear energy loss mechanism, resulting in point defects and clusters. In addition to the separate response to the electronic and the nuclear energy loss, it is important to also understand the response of the material to the combined effects of the electronic and atomic processes. It has been shown that these effects can have additive,[1–7] competing,[8–11] or synergistic[12–16] impacts on damage formation and microstructure alterations. Combining experiment and modeling is necessary to understand such complex behavior and the radiation processes that take place in very short time scales, in order to be able to ultimately predict and control the material's response to the electronic energy deposition. Here, we investigate the variation of electron-phonon coupling on energy dissipation in model oxides with increasing pre-existing disorder, energy deposition to the lattice, and the microstructural response of $SrTiO_3$ and $KTaO_3$ to the dissipation of electronic energy loss (Se) from 21 MeV Ni ions. $SrTiO_3$ and $KTaO_3$ are wide bandgap perovskite-type oxides with applications in a wide variety of fields. $SrTiO_3$ is a material with applications in microelectronics and optoelectronics[17–22] and has a cubic structure above 105 K. $KTaO_3$ is a popular material in ferroelectric applications with a cubic structure that does not undergo a phase transition. Both materials are critical for the functional oxide electronics field.[23–27] We investigate the effects of ion irradiation, as ion beam modification is used to add and control functionality in materials. Ion beam modification has been proposed as an effective tool for tuning the electronic and optical properties of both $SrTiO_3$ and $KTaO_3$. In addition, the configuration of the nanoscale cylindrical structures created by the higher energy ions in predamaged samples leads to unique geometrical functionality that can extend through thin films or layered structures. Therefore, understanding the response of materials to electronic energy loss due to ion irradiation is important.

We use molecular dynamics (MD) simulations combined with the inelastic thermal spike (iTS) model[28] to model the response of $SrTiO_3$ and $KTaO_3$ to the dissipation of electronic energy loss (S_e) from 21 MeV Ni ions. We use pristine systems and systems with different initial disorder levels by introducing a varying amount of

defects. We vary the electron-phonon (e-ph) mean free path to refine previous observations, taking into account the different disorder levels of the initial predamaged states and provide a direct comparison with experiments. The $SrTiO_3$ experiments were performed by predamaging [100]-oriented $SrTiO_3$ single crystal wafers to different relative disorder levels using 900 keV Au ions, as described previously.[13,14] These predamaged samples were subsequently irradiated with 21 MeV Ni ions (S_e = 9.9 keV/nm). Similarly, the $KTaO_3$ experiments were carried out by predamaging [100]-oriented $KTaO_3$ single crystals to different disorder levels using 2 MeV Au ions and then subsequently irradiating the predamaged samples with 21 MeV Ni ions (S_e = 9.2 keV/nm), as described previously.[16] For both materials and all samples, the size of the amorphous ion tracks induced by the electronic energy dissipation was determined from the relative increase in disorder that was characterized by Rutherford backscattering spectrometry along the [100] channeling direction, as described in detail elsewhere.[13,14,16]

The iTS model is a two-temperature model that describes the energy transfer from a fast moving ion to the target material. Energy from the highly energetic ion is transferred to electrons of the target material, increasing their temperature. Energy diffuses from hot to cooler electrons via electron-electron interactions. Consequently, via the e-ph interactions, energy is transferred to the atomic sublattice, where it diffuses among the lattice atoms. The iTS model is used to calculate this energy transfer from the electrons to the atomic system and the deposited energy to the atoms. This energy deposition to the atomic subsystem is used as input in MD simulations, which describes the atomic response to rapid energy transfer due to irradiation. In the iTS model, the energy exchange between the electronic and the atomic subsystems is described via a set of heat diffusion equations. Equation (1) describes the evolution of the electronic temperature, T_e, and Eq. (2) describes the evolution of the atomic temperature, T_a,

$$C_e \frac{\partial T_e}{\partial t} = \frac{1}{r}\frac{\partial}{\partial r}\left[rK_e \frac{\partial T_e}{\partial r}\right] - g(T_e - T_a) + A(r,t), \quad (1)$$

$$C_a \frac{\partial T_a}{\partial t} = \frac{1}{r}\frac{\partial}{\partial r}\left[rK_a \frac{\partial T_a}{\partial r}\right] + g(T_e - T_a). \quad (2)$$

Here, C_e is the specific heat coefficient for the electrons and C_a is the specific heat coefficient for the atomic system. K_e and K_a are the thermal conductivities of the electronic and the atomic systems and g is the e-ph coupling parameter. The term $A(r, t)$ is given by $A(r,t) = bS_e e^{-(t-t_o)^2/2s^2} F(r)$ and describes the energy deposition from the incident ion to the electrons as a Gaussian time distribution and a radial distribution $F(r)$.[29] In this expression, b is the normalization factor that ensures that the integration of $A(r, t)$ is equal to the total electronic energy loss S_e.[30] The parameter s is the half width of the Gaussian distribution, and t_o is of the order of 10^{-15} s.[28] The energy exchange between the two subsystems depends on the temperature difference between them, as expressed by the e-ph coupling parameter on the right-hand side of Eqs. (1) and (2).

The thermal conductivity K_e equals to $C_e \cdot D_e$, with D_e being the thermal diffusivity.[28] The e-ph coupling parameter is related to the e-ph mean free path λ via $g = K_e/\lambda^2$. For the electronic subsystems of pristine $SrTiO_3$ and $KTaO_3$, C_e = 1 J cm^{-3} K^{-1}[28,31] and D_e = 2 J cm^2 s^{-1}. The atomic specific heat, thermal conductivity, and e-ph mean free path for pristine $SrTiO_3$ are C_a = 0.544 J g^{-1} K^{-1}, K_a = 11.2 W m^{-1} K^{-1},[13] and λ = 4.8 nm, respectively. For pristine $KTaO_3$, C_a = 0.375 J g^{-1} K^{-1},[32] K_a = 11 W m^{-1} K^{-1},[33] and λ = 4.9 nm. The e-ph mean free path values for the pristine samples were obtained from Fig. 15 in Ref. 28. As discussed elsewhere,[13,34] the pre-existing irradiation-induced defects result in lower conductivity and smaller values of the e-ph mean free path.[35,36] For the predamaged systems, we reduced K_e and K_a by an order of magnitude and we use different values of e-ph coupling for the different pre-existing disorder levels. Such a decrease in the thermal conductivity is consistent with the large changes in thermal conductivity of $SrTiO_3$ due to processing defects[37] or cation nonstoichiometry (a few percent).[38] The scattering through defects affects the e-ph relaxation time τ, which is proportional to $\frac{1}{g}$, where g is the e-ph coupling parameter. g is proportional to $\frac{1}{\lambda^2}$, meaning that $\tau \sim \lambda^2$. Furthermore, τ is inversely proportional to the number of scattering centers N_c, which means that λ relates to N_c via $\lambda \sim \frac{1}{\sqrt{N_c}}$. The e-ph mean free path can further depend on localized pockets of higher disorder for the systems with higher disorder levels and also on the temperature. The defect density, local disorder pockets, and clusters for higher disorder density and the temperature gradient would contribute to a nonlinear dependency of the mean free path and the measured disorder. We use $SrTiO_3$ systems with about 2% Frenkel pairs (FPs), 4% FPs, 7% FPs, 34% FPs, and 52% FPs with λ values of 2.5 nm, 2.3 nm, 2.2 nm, 1.8 nm, and 1.5 nm, respectively. The values of λ exhibited an exponential dependence on the FP concentration, x, and a curve fitting routine yielded an exponential relation of the form $\lambda = 2.432e^{-0.009x}$. Using this fit, we obtained values of the mean free path 2.35 nm, 2.2 nm, 2 nm, 1.9 nm, and 1.7 nm for $KTaO_3$ systems with about 4%, 11%, 19%, 30%, and 41% FPs, respectively.

For the MD simulations, we used the DL_POLY[39] code. We used empirical potentials[40,41] joined to the ZBL (Ziegler-Biersack-Littmark)[42] repulsive potentials for short distances. The ZBL potential was used for all pair interactions. The systems have a size of about 360 Å × 360 Å × 60 Å. The predamaged systems were created by introducing FPs randomly in the systems, which are then relaxed under constant pressure and temperature, resulting in the disorder mentioned above. The simulated irradiation was performed under the NVE ensemble along the z direction of the MD box with a variable timestep. The velocities of atoms within a 10 Å layer in the x and y dimensions of the box are scaled to 300 K according to a Gaussian distribution to emulate the bulk. The sphere criterion is used to identify the defects[43] with a cut-off radius of 0.75 Å.

Figure 1 shows thermal spike calculations of the maximum lattice temperature profiles for a 21 MeV Ni ion as a function of the radial distance from the ion path in $SrTiO_3$ and $KTaO_3$. The profiles in Fig. 1(a) correspond to irradiation of a pristine crystalline $SrTiO_3$ system and predamaged $SrTiO_3$ systems with 2% FPs, 4% FPs, 7% FPs, 34% FPs, and 52% FPs. In Fig. 1(b), the maximum lattice temperature for irradiation of pristine crystalline $KTaO_3$ and predamaged $KTaO_3$ with 4% FPs, 11% FPs, 19% FPs, 30% FPs and 34% FPs is shown. As the initial pre-existing disorder increases, the defects act as scattering centers resulting in shorter e-ph mean free paths. This means that the phonons interact faster with the hot electrons, resulting in the development of higher temperature in the vicinity of the ion path.

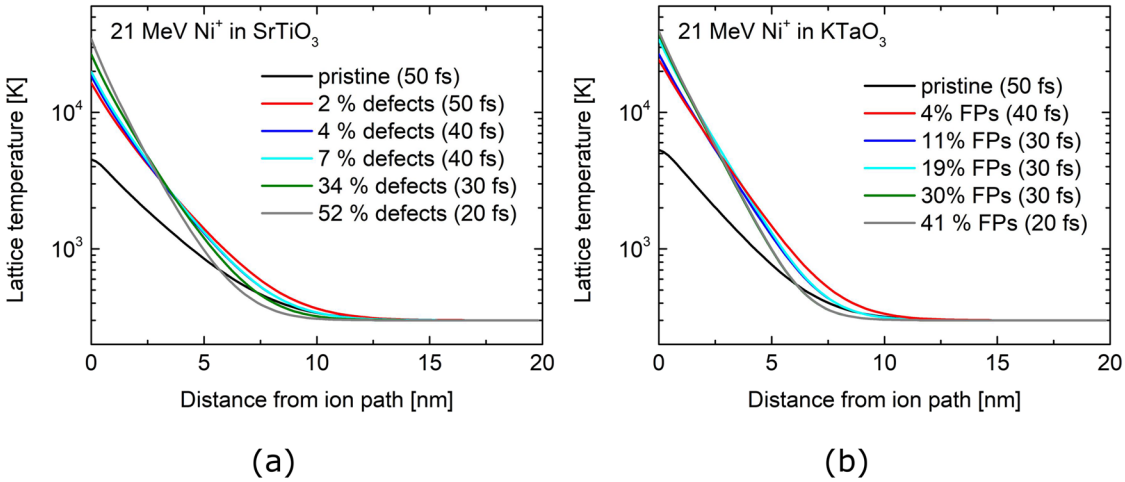

FIG. 1. Thermal spike calculations of the maximum lattice temperature profiles as a function of the radial distance from the ion path due to 21 MeV Ni ion irradiation in pristine and predamaged (a) $SrTiO_3$ and (b) $KTaO_3$ systems. The corresponding time of each profile is given in brackets.

The energy deposition profiles that correspond to the lattice temperature profiles shown in Fig. 1 are used as input in MD simulations of irradiation. We ran six irradiation simulations for $SrTiO_3$ and four for $KTaO_3$. For comparison, we plotted the lattice temperature samples with intermediate pre-existing disorder ($KTaO_3$ with 11% FPs and $SrTiO_3$ with 7% FPs from Fig. 1) in Fig. 2(a). Figure 2(b) shows the energy deposition profiles that correspond to these temperature profiles, as a function of the distance from the ion path. As seen here, the lattice temperature for 7% predamaged $SrTiO_3$ is smaller than the one for 11% predamaged $KTaO_3$, and the corresponding deposited energy per atom is the same for the two systems.

Figures 2(c) and 2(d) show the amorphous ion tracks formed in predamaged $SrTiO_3$ and $KTaO_3$ due to the energy deposition profiles shown in Fig. 2(b). The cross sections shown here have size 100 Å × 100 Å, and the diameters of the tracks are 4.1 ± 0.1 nm and 3.5 ± 0.1 nm for $SrTiO_3$ and $KTaO_3$, respectively. For the same energy deposition, the ion track in $SrTiO_3$ is larger compared to the one in $KTaO_3$. The smaller track in $KTaO_3$ compared to $SrTiO_3$ can be attributed to the different amorphization and recrystallization behavior of the two perovskites. This trend, smaller tracks in $KTaO_3$ than in $SrTiO_3$, is shown in Fig. 3(a) for all the MD simulations of 21 MeV Ni irradiation. Figure 3(b) shows previously reported[13,14,16] and unreported experimental results on ion track size for different initial disorder levels. For high initial disorder levels, the defect pockets are more dense and larger, resulting in larger size difference between the tracks in the two materials, on the order of 2 nm difference, compared to low disorder levels, such as in the case shown in Fig. 2, where the track size difference is of the order of 0.5 nm.

Figures 3(a) and 3(b) show the dependence of ion track size on initial disorder. While increasing track size with increasing disorder was also observed for constant value of the e-ph mean free path,[34] this work provides better agreement with the experimental trends than previously when a constant value was assumed. These new values are very important for defining the appropriate values of the mean free path with changes in disorder or defect concentration, which provides deeper understanding of the role of the defects on the energy dissipation and microstructure alterations. For the low initial disorder level, there is a linear dependence of the track size on the pre-existing level of defects in $SrTiO_3$, both in MD and in the experiments. As the initial concentration of defects reaches nearly 50% in $SrTiO_3$, the track size saturates. Similarly, for increasing level or pre-existing defects, the track size increases in $KTaO_3$. As the disorder level increases, the track diameter size starts saturating. As seen here, the MD simulations are consistent with the experimental behavior. Discrepancy in the track size between MD and experiment can be attributed to several reasons. First, the exact measurement of disorder in terms of FPs is not possible experimentally. Second, the FPs concentration is measured over the MD cell, while the initial experimental disorder is measured by ion channeling and is only proportional to the relative Sr and Ta defect concentrations. Experimentally, the defect structure introduced consists of point defects and small defect clusters, as well as amorphous domains at higher disorder levels. Unfortunately, we do not know the nature and size distribution of these defects, since they are not readily observed in HRTEM. Additionally, the MD measurements are an average of measurements along one track, while the experimental values are an average of a large number of tracks. Of course, the empirical potential may not accurately describe melting and atomic response over the range of FP concentrations. Finally, the e-ph mean free path cannot be calculated exactly. While the presence of the defects result in the reduced e-ph mean free path, as discussed earlier, accurate measurements of the e-ph mean free path are not possible. Here, by taking this effect into consideration, it is shown that the defects play a significant role in the energy dissipation and the atomic response to rapid energy deposition due to irradiation. Understanding the role of the defects is necessary for predicting the material's behavior and for inducing desired microstructure alterations.

To further investigate the behavior of the predamaged $SrTiO_3$ and $KTaO_3$, particularly the response to heat and the melting of

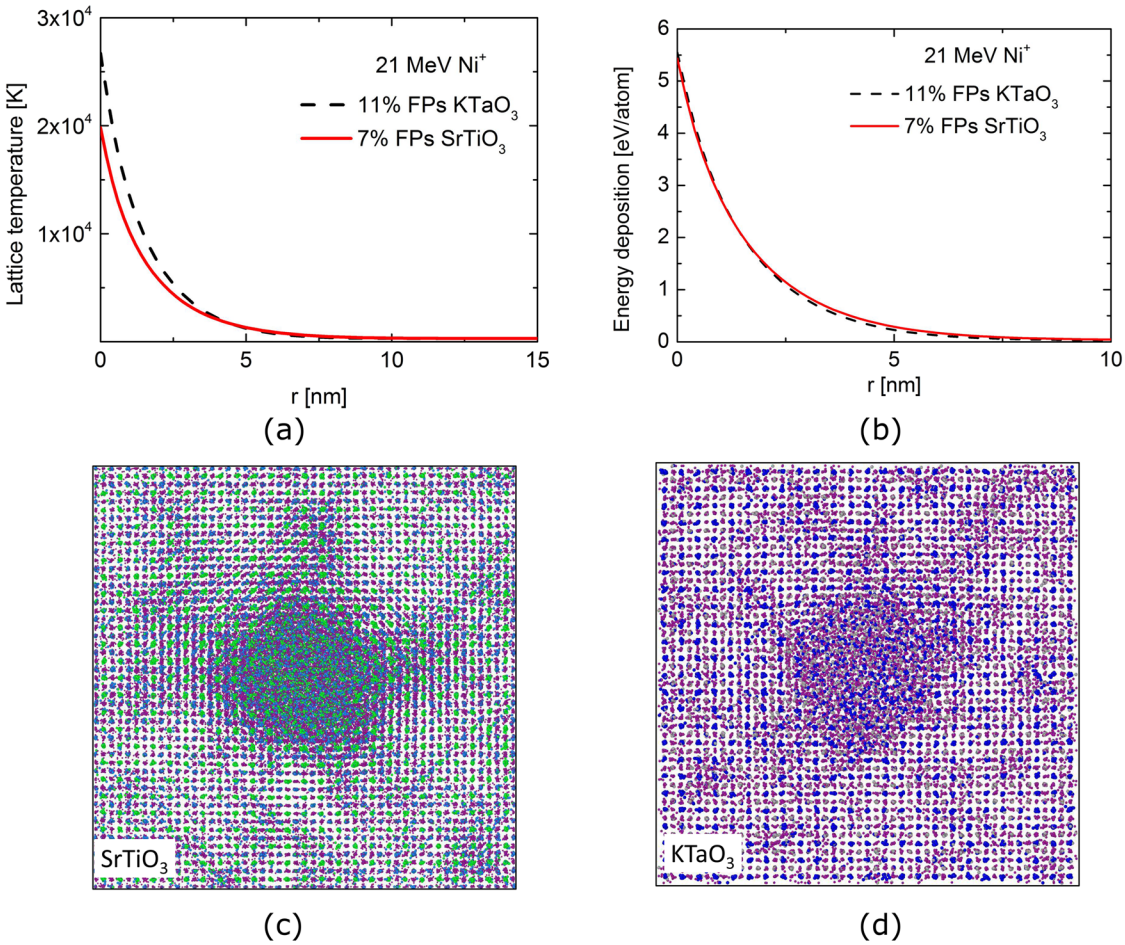

FIG. 2. (a) Maximum lattice temperature profiles due to 21 MeV Ni irradiation of predamaged $SrTiO_3$ with 7% FPs and predamaged $KTaO_3$ with 11% FPs, as a function of the distance from the ion path. (b) Corresponding energy deposition profiles in eV/atom. Cross section of (c) a $SrTiO_3$ system with 7% FPs pre-existing disorder and (d) a $KTaO_3$ system with 11% FPs pre-existing disorder after a thermal spike of 21 MeV Ni ion. The area shown is 100 Å × 100 Å. Sr is shown in blue, Ti in green, K in dark blue, Ta in gray, and O in purple.

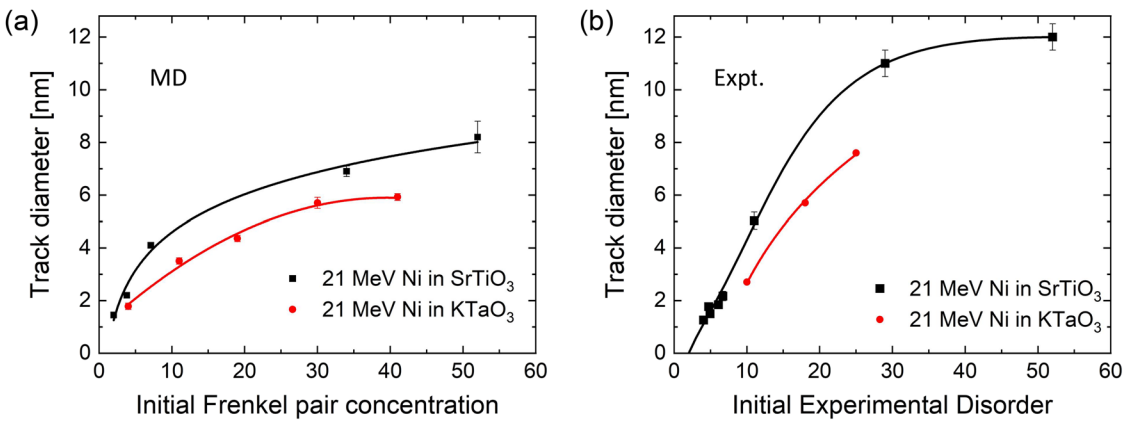

FIG. 3. (a) Ion track diameter for MD simulations of 21 MeV Ni ion irradiation of predamaged $SrTiO_3$ and $KTaO_3$ as a function of initial Frenkel pair concentration. The error bars represent the standard deviation over different measurements of the diameter along one ion track in each system. (b) Previously reported[13,14,16] and unreported experimental determinations of ion track sizes due to 21 MeV Ni ion irradiation of predamaged $SrTiO_3$ and $KTaO_3$ (the error bars are discussed in Ref. 13).

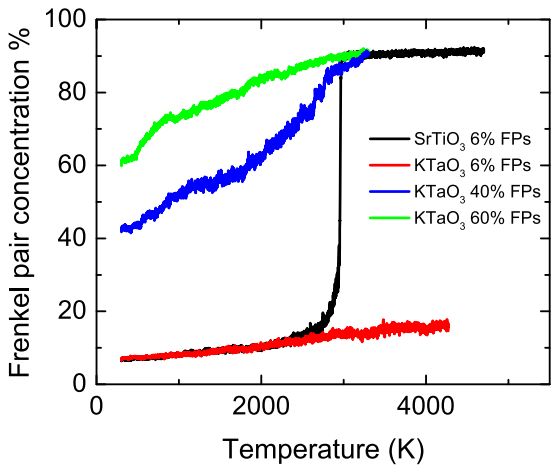

FIG. 4. Evolution of defect concentration for increasing temperature with rate 1 K/ps for a $SrTiO_3$ sample with 6% pre-existing FPs (green line) and $KTaO_3$ samples with 6%, 40%, and 60% pre-existing FPs (red, blue, and green lines, respectively).

the materials, we investigated the behavior of predamaged samples for increasing temperature, with 1 K/ps rate. $SrTiO_3$ and $KTaO_3$ samples with 6% pre-existing FPs were heated to temperatures well above their melting point (2353 K for $SrTiO_3$ and 1625 K for $KTaO_3$). As shown in Fig. 4, melting of $SrTiO_3$ is observed when the melting temperature is reached, while the number of FPs increases with temperature for $KTaO_3$ without melting (black and red lines, respectively). The same heating rate was applied for the $KTaO_3$ samples with 40% and 60% pre-existing FPs. As described in Fig. 4 by the blue and green lines, both samples reach about 92%, which means that the samples are amorphous. This shows that amorphization of $KTaO_3$ depends on the predamage level. This behavior shows the more complex behavior of amorphization of $KTaO_3$, which has been previously observed in ion irradiation experiments[44–46] and explains the difference in the track size.

Overall, the description of the response of pristine and predamaged $SrTiO_3$ and $KTaO_3$ to 21 MeV Ni ions using a combination of the iTS and MD simulations agrees well with experiments. We have shown that the initial disorder affects the e-ph mean free path and the energy dissipation, and therefore the energy deposition to the atoms. While the defects are usually considered unwanted damage, they can be used to manipulate the materials' behavior. More accurate values of the e-ph coupling parameter obtained with first principle calculations could improve the agreement between the predicted track size by MD and the experimentally determined track size, but they are not currently available. This work emphasizes the importance of combining modeling and experiments both for understanding and predicting the materials' behavior under irradiation. Investigation of the synergistic effects of the pre-existing disorder and the electronic energy loss is need in more materials and for different ions and energies in order to understand the radiation damage processes that take place in such short time scales.

This work was supported by the U.S. Department of Energy, Office of Science, Basic Energy Sciences, Materials Sciences and Engineering Division. This research used resources of the National Energy Research Scientific Computing Center, supported by the Office of Science, U.S. Department of Energy under Contract No. DEAC02-05CH11231.

This manuscript has been authored by UT-Battelle, LLC under Contract No. DE-AC05-00OR22725 with the U.S. Department of Energy. The United States Government retains and the publisher, by accepting the article for publication, acknowledges that the United States Government retains a non-exclusive, paid-up, irrevocable, world-wide license to publish or reproduce the published form of this manuscript, or allow others to do so, for United States Government purposes. The Department of Energy will provide public access to these results of federally sponsored research in accordance with the DOE Public Access Plan (http://energy.gov/downloads/doe-public-access-plan).

REFERENCES

[1] M. Toulemonde, W. J. Weber, G. Li, V. Shutthanandan, P. Kluth, T. Yang, Y. Wang, and Y. Zhang, Phys. Rev. B **83**, 054106 (2011).
[2] L. Thomé, A. Debelle, F. Garrido, P. Trocellier, Y. Serruys, G. Velisa, and S. Miro, Appl. Phys. Lett. **102**, 141906 (2013).
[3] M. Sall, I. Monnet, C. Grygiel, B. Ban d'Etat, H. Lebius, S. Leclerc, and E. Balanzat, Europhys. Lett. **102**, 26002 (2013).
[4] Y. Zhang, D. S. Aidhy, T. Varga, S. Moll, P. D. Edmondson, F. Namavar, K. Jin, C. N. Ostrouchov, and W. J. Weber, Phys. Chem. Chem. Phys. **16**, 8051–8059 (2014).
[5] Y. Y. Wang, C. Grygiel, C. Dufour, J. R. Sun, Z. G. Wang, Y. T. Zhao, G. Q. Xiao, R. Cheng, X. M. Zhou, J. R. Ren, S. D. Liu, Y. Lei, Y. B. Sun, R. Ritter, E. Gruber, A. Cassimi, I. Monnet, S. Bouffard, F. Aumayr, and M. Toulemonde, Sci. Rep. **4**, 5742 (2014).
[6] M. Backman, F. Djurabekova, O. H. Pakarinen, K. Nordlund, Y. Zhang, M. Toulemonde, and W. J. Weber, J. Phys. D: Appl. Phys. **45**, 505305 (2012).
[7] E. Zarkadoula, M. Toulemonde, and W. J. Weber, Appl. Phys. Lett. **107**, 261902 (2015).
[8] A. Debelle, M. Backman, L. Thomé, W. J. Weber, M. Toulemonde, S. Mylonas, A. Boulle, O. H. Pakarinen, N. Juslin, F. Djurabekova, K. Nordlund, F. Garrido, and D. Chaussende, Phys. Rev. B **86**, 100102 (2012).
[9] W. J. Weber, Y. Zhang, H. Y. Xiao, and L. M. Wang, RSC Adv. **2**, 595–604 (2012).
[10] Y. Zhang, T. Varga, M. Ishimaru, P. D. Edmondson, H. Xue, P. Liu, S. Moll, F. Namavar, C. Hardiman, S. Shannon, and W. J. Weber, Nucl. Instrum. Methods Phys. Res., Sect. B **327**, 33–43 (2014).
[11] W. J. Weber, H. Xue, E. Zarkadoula, and Y. Zhang, Scr. Mater. **173**, 154–157 (2019).
[12] A. Kamarou, W. Wesch, and E. Wendler, Phys. Rev. B **78**, 054111 (2008).
[13] W. J. Weber, E. Zarkadoula, O. H. Pakarinen, R. Sachan, M. F. Chisholm, P. Liu, H. Xue, K. Jin, and Y. Zhang, Sci. Rep. **5**, 7726 (2015).
[14] H. Xue, E. Zarkadoula, R. Sachan, Y. Zhang, C. Trautmann, and W. J. Weber, Acta Mater. **150**, 351–359 (2018).
[15] E. Zarkadoula, K. Jin, Y. Zhang, and W. J. Weber, AIP Adv. **7**, 015016 (2017).
[16] K. Jin, Y. Zhang, and W. J. Weber, Mater. Res. Lett. **6**, 531–536 (2018).
[17] K. Oyoshi, S. Hishita, and H. Haneda, J. Appl. Phys. **87**, 3450–3456 (2000).
[18] G. D. Wilk, R. M. Wallace, and J. M. Anthony, J. Appl. Phys. **89**, 5243–5275 (2001).
[19] N. Erdman, K. R. Poeppelmeler, M. Asta, O. Warschkow, D. E. Ellis, and L. D. Marks, Nature **419**, 55 (2002).
[20] A. Kosola, M. Putkonen, L. S. Johansson, and L. Niinisto, Appl. Surf. Sci. **211**, 102–112 (2003).
[21] J. H. Haeni, P. Irvin, W. Chang, R. Uecker, P. Reiche, Y. L. Li, S. Choudhury, W. Tian, M. E. Hawley, B. Craigo, A. K. Tagantsev, X. Q. Pan, S. K. Streiffer, L. Q. Chen, S. W. Kirchoefer, J. Levy, and D. G. Schlom, Nature **430**, 758–761 (2004).

[22] A. Spinelli, M. A. Torija, C. Liu, C. Jan, and C. Leighton, Phys. Rev. B **81**, 155110 (2010).
[23] A. R. Benrekia, N. Benkhettou, A. Nassour, M. Driz, M. Sahnoun, and S. Lebegue, Physica B **407**, 2632 (2012).
[24] W. D. Rice, P. Ambwani, M. Bombeck, J. D. Thompson, G. Haugstad, C. Leighton, and S. A. Crooker, Nat. Mater. **13**, 481–487 (2014).
[25] K. Zou, S. Ismail-Beigi, K. Kisslinger, X. Shen, D. Su, F. J. Walker, and C. H. Ahn, APL Mater. **3**, 036104 (2015).
[26] Y. Yang, C. S. Lin, and W. D. Cheng, AIP Adv. **5**, 057147 (2015).
[27] P. Sharma, Z. Huang, M. Li, C. Li, S. Hu, H. Lee, J.-W. Lee, C.-B. Eom, S. J. Pennycook, J. Seidel, Ariando, and A. Gruverman, Adv. Funct. Mater. **28**, 1707159 (2018).
[28] M. Toulemonde, W. Assman, C. Dufour, A. Meftah, F. Studer, and C. Trautmann, Mat. Fys. Medd. K. Dan. Vidensk. Selsk. **52**, 263–292 (2006).
[29] M. P. R. Waligorski, R. N. Hamm, and R. Katz, Nucl. Tracks Radiat. Meas. **11**, 309–319 (1986).
[30] C. Dufour, A. Audouard, F. Beuneu, J. Dural, J. P. Girard, A. Hairie, M. Levalois, E. Paumier, and M. Toulemonde, J. Phys.: Condens. Matter **5**, 4573–4584 (1993).
[31] A. Meftah, J. M. Costantini, N. Khalfaoui, S. Boudjadar, J. P. Stoquert, F. Studer, and M. Toulemonde, Nucl. Instrum. Methods Phys. Res., Sect. B **237**, 563–574 (2005).
[32] X. P. Wang, J. Y. Wang, H. J. Zhang, Y. G. Yu, J. Wu, W. L. Gao, and R. I. Boughton, J. Appl. Phys. **103**, 033513 (2008).
[33] M. Tachibana, T. Kolodiazhnyi, and E. Takayama-Muromachi, Appl. Phys. Lett. **93**, 092902 (2008).
[34] E. Zarkadoula, H. Xue, Y. Zhang, and W. J. Weber, Phys. Chem. Chem. Phys. **17**, 22538–22542 (2015).
[35] L. L. Snead, S. J. Zinkle, and D. P. White, J. Nucl. Mater. **340**, 187–202 (2005).
[36] P. B. Weisensee, J. P. Feser, and D. G. Cahill, J. Nucl. Mater. **443**, 212–217 (2013).
[37] D.-W. Oh, J. Ravichandran, C.-W. Liang, W. Siemons, B. Jalan, C. M. Brooks, M. Huijben, D. G. Schlom, S. Stemmer, L. W. Martin, A. Majumdar, R. Ramesh, and D. G. Cahill, Appl. Phys. Lett. **98**, 221904 (2011).
[38] E. Breckenfeld, R. Wilson, J. Karthik, A. R. Damodaran, D. G. Cahill, and L. W. Martin, Chem. Mater. **24**, 331–337 (2012).
[39] I. T. Todorov, B. Smith, M. T. Dove, and K. Trachenko, J. Mater. Chem. **16**, 1911 (2006).
[40] M. A. McCoy, R. W. Grimes, and W. E. Lee, Philos. Mag. A **75**, 833–846 (1997).
[41] M. Exner, H. Donnerberg, C. R. A. Catlow, and O. F. Schirmer, Phys. Rev. B **52**, 3930 (1995).
[42] J. F. Ziegler, J. P. Biersack, and U. Littmark, *The Stopping and Range of Ions in Matter* (Pergamon, New York, 1985).
[43] I. T. Todorov and W. Smith, The DL Poly 4 User Manual, v. 4, www.ccp5.ac.uk/DL_POLY/MANUALS/USRMAN4.pdf (2012).
[44] C. W. White, C. J. McHargue, P. S. Sklad, L. A. Boatner, and C. G. Farlow, Mater. Sci. Rep. **4**, 41 (1989).
[45] A. Meldrum, L. A. Boatner, W. J. Weber, and R. C. Ewing, J. Nucl. Mater. **300**, 242–254 (2002).
[46] A. Meldrum, L. A. Boatner, and R. C. Ewing, "Temperature-induced phase transitions during ion-beam irradiation of the perovskite-structure oxides," UNT Digital Library, Tennessee, http://digital.library.unat.edu/ark:/67531/metadc691312/.